

Quantifying water cover shifts across the globe: following the steps of walking floods

P. Torre Zaffaroni^{1,2,3}, J. Houspanossian³, C.M. Di Bella^{1,2}, E.G. Jobbágy³

¹ Instituto de Investigaciones Fisiológicas y Ecológicas Vinculadas a la Agricultura (IFEVA), Facultad de Agronomía, Universidad de Buenos Aires, CONICET, Buenos Aires, Argentina

² Departamento de Métodos Cuantitativos y Sistemas de Información, Facultad de Agronomía, Universidad de Buenos Aires, Argentina

³ Grupo de Estudios Ambientales — IMASL, Universidad Nacional de San Luis & CONICET, San Luis, Argentina

Contents of this file

Text S1

Figures S1 to S6

Text S1.

Attribution of displacement to natural and induced factors

One way to test the influence of multiple continuous variables that might have interactive and/or non-linear effects is through boosted regression trees, which are based on machine learning algorithms capable of determining features' importance while maintaining adequate interpretability (Elith et al., 2008; Radinger et al., 2018). Based on the effect of topography on potential energy guiding the stagnancy of surface water, and of climate regimes in terms of spatial variability of rainfall events, we hypothesized that (1) displacement is fostered by low water convergence, which could be the result of largely flat topographies, highly meandering rivers, increasing aridity. Based on the different allocation of flooding for crops, decoupled from how flooding spreads over a floodplain, and the long-term effect of dam emplacement on the local flooding regime of the altered water course, we further hypothesize that (2) flooding displacement is enhanced by intensely irrigated regions destined to rice production and countered by well-defined lakes, including natural formations and manmade dams and emplacements for storing water.

We selected global datasets related to some of the most relevant aspects in which flooding displacement may be influenced by topography, climate, and large-scale anthropic activity. Figure S1 gathers the geographical distribution of these variables aggregated to each landscape. We obtained information from (1) Global Multi-resolution Terrain Elevation Data (GMTED2010, USGS) to derive three topographical variables: (a) terrain ruggedness (Riley et al., 1999), and slope integrated at (b) local (250m) and (c) regional (5km) levels (Figure S1 a-b); (2) Global database of river width, slope, catchment area, meander wavelength, sinuosity, and discharge (Frasson et al., 2019, and based upon Global River Width from Landsat, Allen & Pavelsky 2018) to derive the average meander wavelength across all riverine segments (between 60°N and 56°S) contained in each landscape (Figure S1c); (3) Global Lake and Wetlands Dataset (GLWD; Lehner & Doll 2004) to derive four hydrological variables: lake, river, floodplain and reservoir coverage fractions per landscape (Figure S1 d-g); (4) TerraClimate (Abatzoglou et al., 2018) to derive the climatological aridity index as the long-term of annual precipitation-to-potential evapotranspiration ratio (Figure S1h); (5) 2015 Anthromes 12K (Ellis et al., 2019) from which we derived three agricultural variables related with water management: rice, irrigated and rainfed coverage fractions per landscape (Figure S1 i-k). We also included the fraction covered by remote woodlands and flooded forests (Figure S1 l-m) as a proxy of one key passive satellite data caveat which can interfere with the depiction of surface water observation by remote sensors onboard satellite platforms.

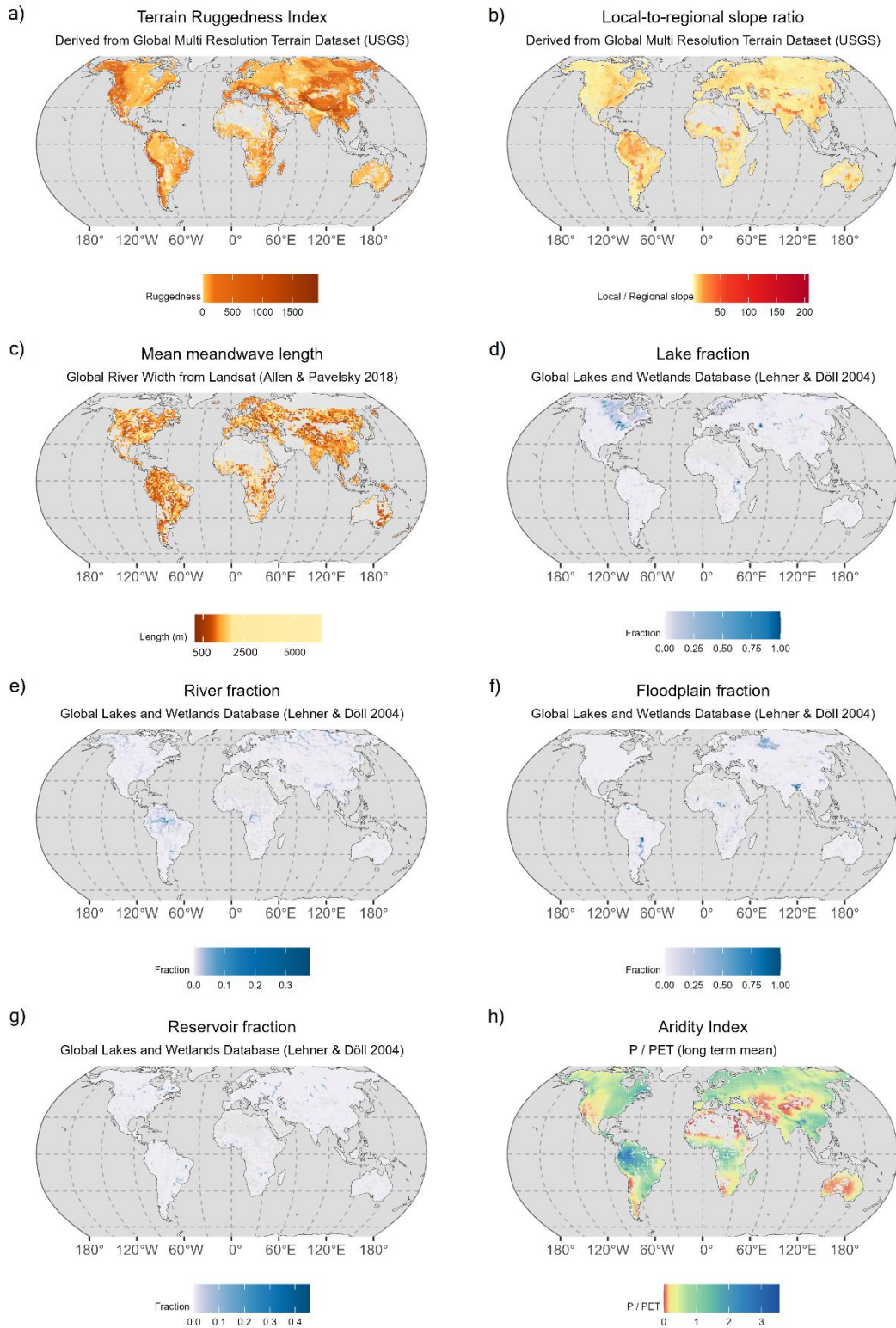


Figure S1. Geographical distribution of the thirteen variables for which we analyzed their influence on flooding displacement: (a) Terrain Ruggedness Index; (b) Local-to-Regional slope ratio; (c) Mean meandwave length; (d) Lake fraction; (e) River fraction; (f) Floodplain fraction; (g) Reservoir fraction; (h) Aridity Index.

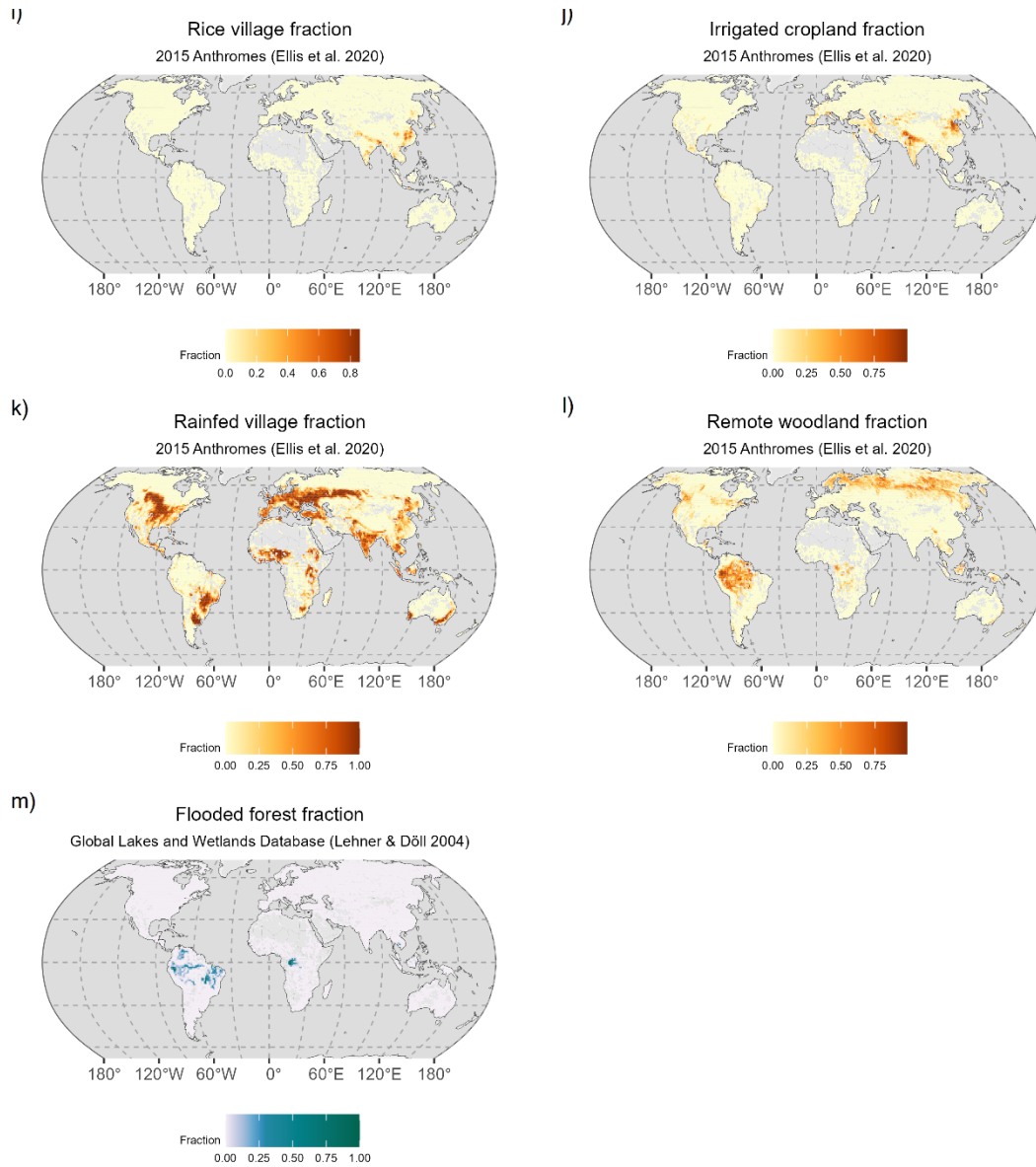


Figure S1 (cont.). Geographical distribution of the thirteen variables for which we analyzed their influence on flooding displacement: (i) Rice fraction; (j) Irrigated cropland fraction; (k) Rainfed fraction; (l) Remote woodland fraction; (m) Flooded forest fraction.

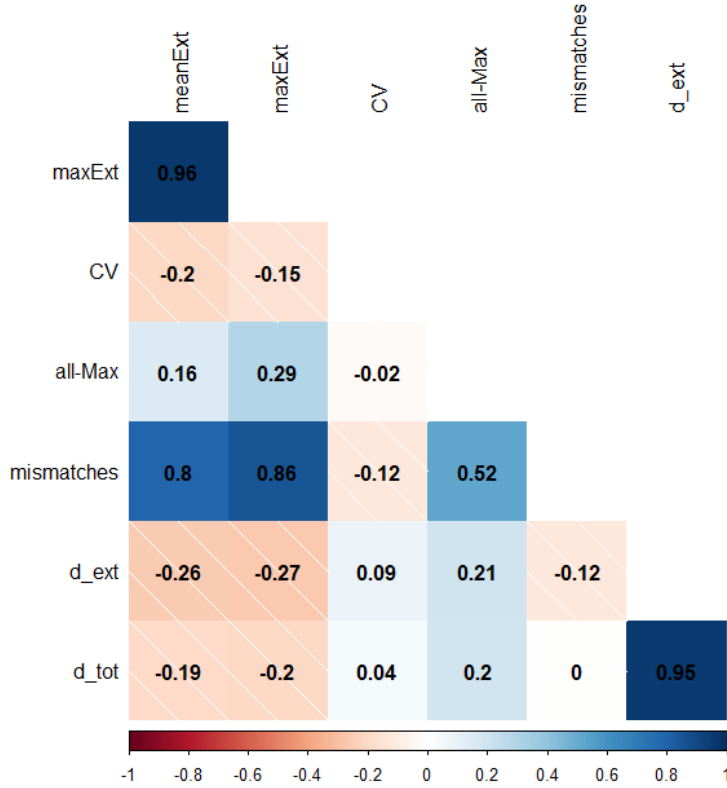


Figure S2. Correlation matrix of typical flooding descriptors and proposed indicators of flooding displacement, all derived from the same dataset (monthly, Landsat-based Global Surface Water; Pekel et al., 2016). Color hue reflects the direction of Spearman’s rho correlation (red = negative; blue = positive), while color intensity reflects the strength of the correlation. maxExt = maximum registered flooded extent per 1-degree grid cell at any month between 1985 and 2020; CV = coefficient of variation (mean / sd); all-Max = absolute difference between the sum of all pixels having been flooded at any point between 1985 and 2020, and the maximum registered flooded event (maxExt); mismatches = absolute differences between the null model of coherent flooding development and the actual, pixel-level flooding frequency distribution; d_ext = extreme displacement index (Eq. 1); d_tot = total displacement index (Eq. 2).

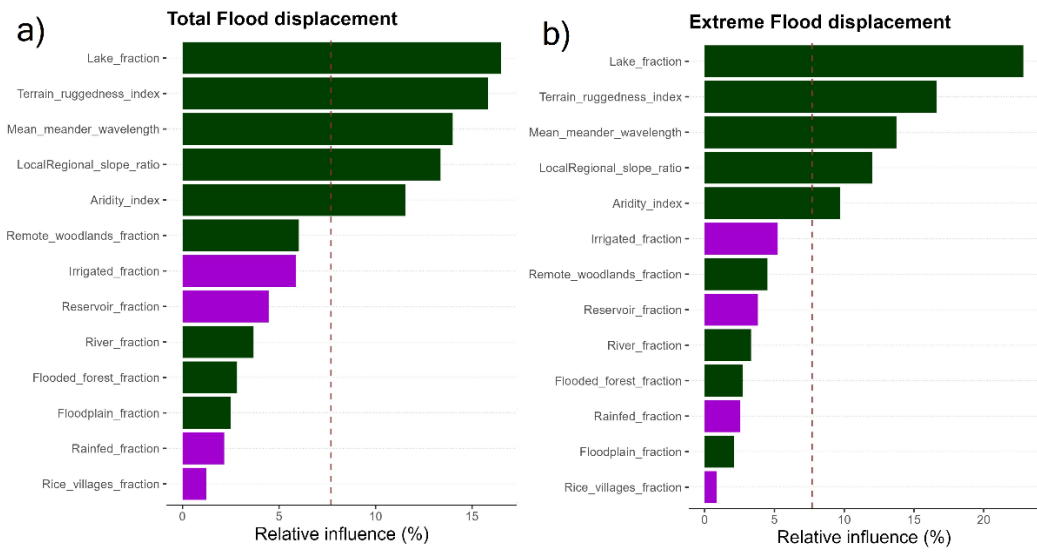


Figure S3. Natural (green) and human (violet) relative influences on (a) total and (b) extreme flooding displacement. Influence values are averaged across a thousand regression tree iterations.

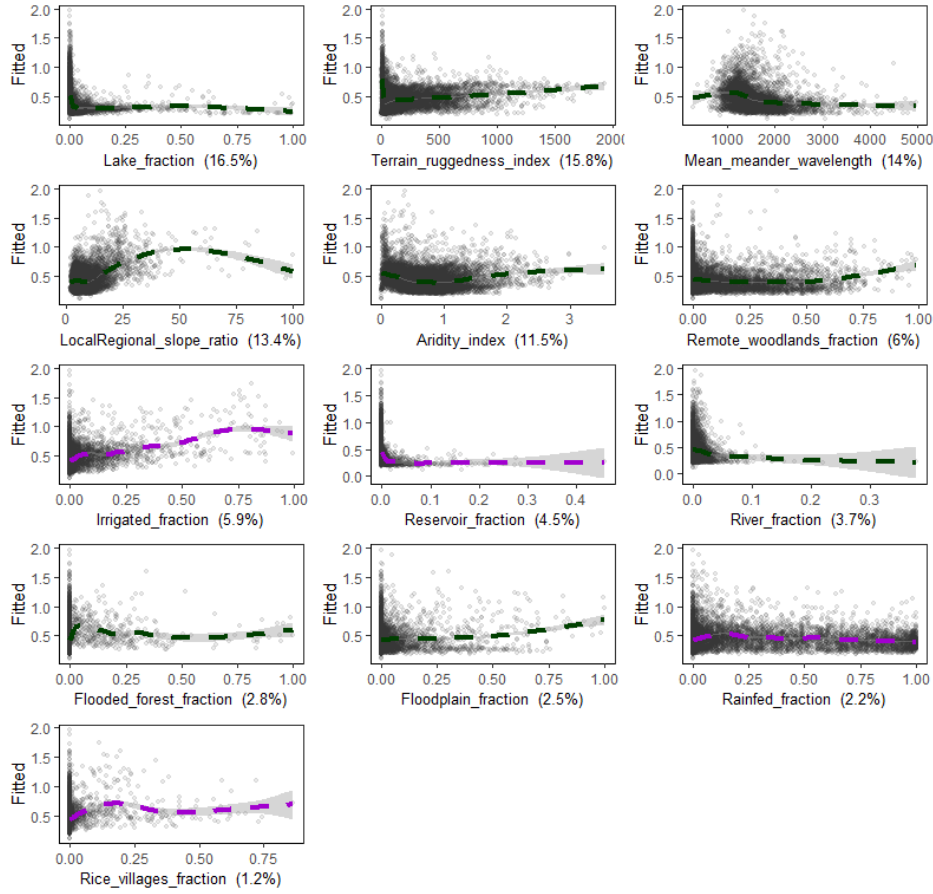


Figure S4. Marginal effect of the natural and induced factors of total flooding displacement (d_{tot}), fitted through general additive models (gam). Values between parenthesis at the x-axis correspond to the relative influence of each variable (averaged across 1000 iterations).

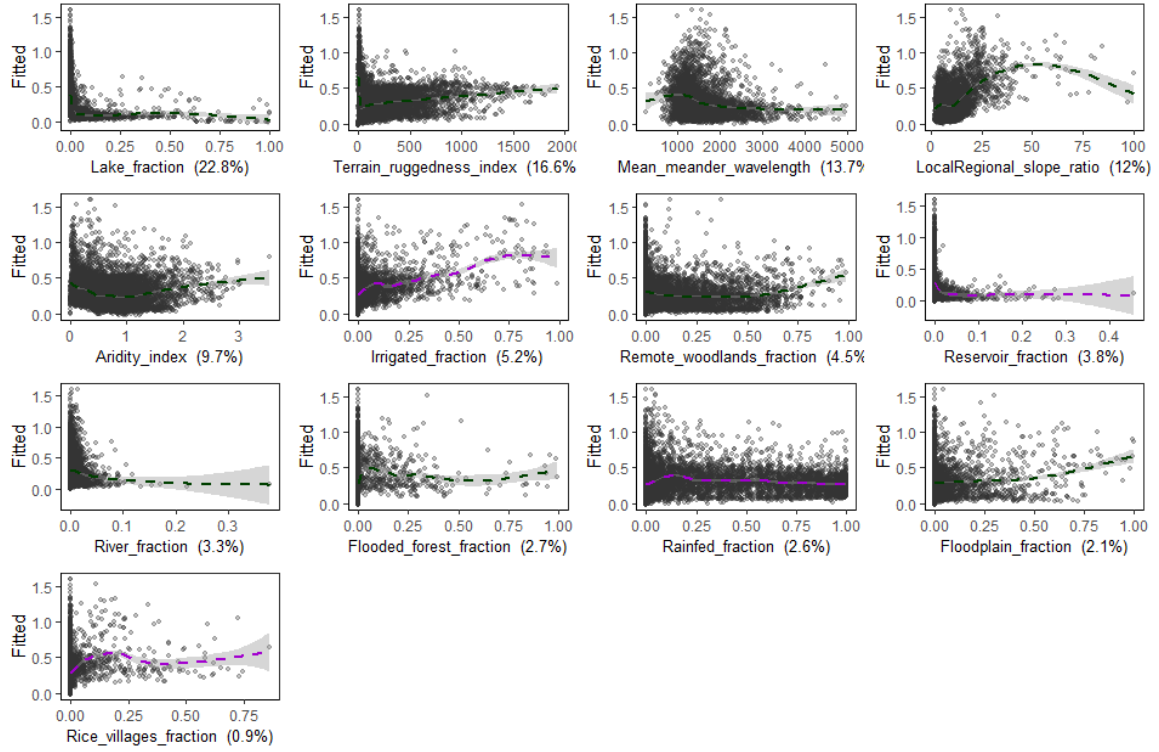


Figure S5. Marginal effect of the natural and induced factors of extreme flooding displacement (d_{ext}), fitted through general additive models (gam). Values between parenthesis at the x-axis correspond to the relative influence of each variable (averaged across 1000 iterations).

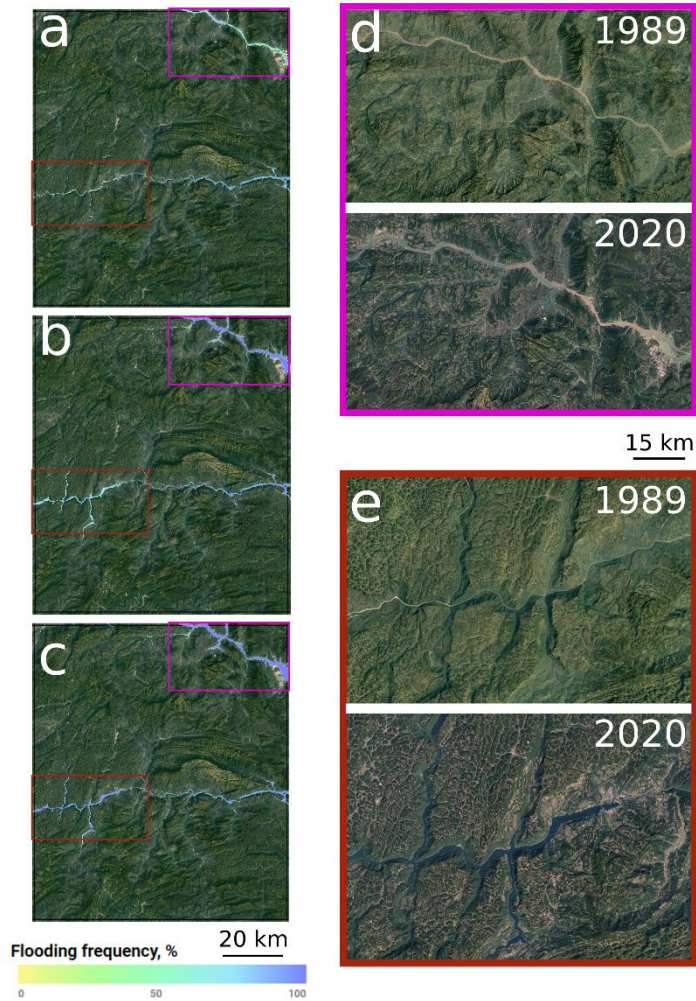


Figure S6. Example of displacement reduction as a result of water reservoir emplacement in a 1°x1° landscape centered at 30.5°N, 110.5°E encompassing the Three Gorges Dam (magenta box) and Shuibuiya Dam (red box) which were built and put into operation between 1994 and 2008. (a-c) geographical distribution of flooding frequency for the periods 1985-2002 (i.e., before the operation of either dam); 2003-2021 (i.e., operational period of the TGD but not SD); and 2009-2021 (i.e., operational period of both dams). (d-e) comparative Google Earth images over the Yangtze River and Qingjiang River, respectively, before and after the emplacement of the dams.

References

- Abatzoglou, J. T., Dobrowski, S. Z., Parks, S. A., & Hegewisch, K. C. (2018). *Terraclimate: Monthly climate and climatic water balance for global terrestrial surfaces, university of idaho* [dataset]. Retrieved from https://developers.google.com/earth-engine/datasets/catalog/IDAHO_EPSCOR_TERRACLIMATE doi: 10.1038/sdata.2017.191
- Allen, G. H., & Pavelsky, T. (2018). Global extent of rivers and streams. *Science*, 361 (6402), 585–588. doi: 10.1126/science.aat063
- Elith, J., Leathwick, J. R., & Hastie, T. (2008). *A working guide to boosted regression trees* (Vol. 77) (No. 4). John Wiley & Sons, Ltd. doi: 10.1111/j.1365-2656.2008.01390.x
- Ellis, E., & Klein Goldewijk, K. (2019). *Anthromes 12k full dataset* [dataset]. Retrieved from <https://dataverse.harvard.edu/dataset.xhtml?persistentId=doi:10.7910/DVN/G0QDNQ> doi: 10.7910/DVN/G0QDNQ
- Frasson, R. P. d. M., Pavelsky, T. M., Fonstad, M. A., Durand, M. T., Allen, G. H., Schumann, G., . . . Yang, X. (2019). *Global database of river width, slope, catchment area, meander wavelength, sinuosity, and discharge* [dataset]. Zenodo. Retrieved from <https://doi.org/10.5281/zenodo.2582500> doi: 10.5281/zenodo.2582500
- Lehner, B., & Döll, P. (2004). *Global lakes and wetlands database: Lakes and wetlands grid (level 3)* [dataset]. World Wildlife Fund. Retrieved from <https://www.worldwildlife.org/publications/global-lakes-and-wetlands-database-lakes-and-wetlands-grid-level-3>
- Pekel, J.-F., Cottam, A., Gorelick, N., & Belward, A. S. (2016a). High-resolution mapping of global surface water and its long-term changes. *Nature*, 540 (7633), 418–422. doi: 10.1038/nature2058
- Radinger, J., Alcaraz-Hernández, J. D., & García-Berthou, E. (2018). *Environmental and spatial correlates of hydrologic alteration in a large Mediterranean river catchment*. *Science of The Total Environment*, 639, 1138–1147. doi: 10.1016/J.SCITOTENV.2018.05.227
- Riley, S., DeGloria, S., & Elliot, R. (1999). *A terrain ruggedness that quantifies topographic heterogeneity*. *Intermountain Journal of Science*, 5 (1-4), 23–27